Proc. Natl. Acad. Sci. USA
Vol. 88, pp. 6418–6422, August 1991
Biophysics

A molecular blueprint for the pore-forming structure of voltage-gated calcium channels

(drug/lipid bilayers/molecular modeling/four-helix bundle)

ANNE GROVE*, JOHN M. TOMICH†, AND MAURICIO MONTAL*‡

*Departments of Biology and Physics, University of California San Diego, La Jolla, CA 92093-0319; and †Department of Biochemistry, University of Southern California Medical School and Children's Hospital, Los Angeles, CA 90054-0700

Communicated by Joseph Kraut, May 8, 1991 (received for review April 11, 1991)

ABSTRACT **A protein that imitates the sequence of a highly conserved segment predicted to line the pore of dihydropyridine-sensitive L-type calcium channels was designed and synthesized. Single-channel conductance properties were studied in planar lipid bilayers. The synthetic protein emulates the ionic conductance, ionic selectivity, and pharmacological properties of the authentic calcium channel, including the stereospecific action of agonist and antagonist enantiomers of the dihydropyridine BayK 8644. The identified sequence is identical in L-type calcium channels from skeletal muscle and isoforms of cardiac muscle, brain, and aorta. It is plausible that this structural motif represents the molecular blueprint for the pore-forming structure of voltage-gated calcium channels.**

Voltage-sensitive calcium channels play a key regulatory role in cell biology as effectors of several signaling processes and targets of a variety of drugs and toxins that alter the physiology of the cell by modulating calcium flow (1, 2). Modulators of the L-type calcium channels include the 1,4-dihydropyridines (DHPs), which are of immense therapeutic value (3).

The DHP-sensitive calcium channel from skeletal muscle is composed of five subunits (4–7), α_1, α_2, β, γ, and δ, with the α_1 subunit forming a functional voltage-gated calcium channel (8–10). Primary structures of the α_1 subunit of the DHP receptor from skeletal (11) and cardiac (8) muscle, brain (12), aorta (13), and lung (14) were elucidated. The amino acid sequence of calcium- and sodium-channel proteins, which show extensive homology, suggests the occurrence of four homologous domains (I–IV) organized as pseudosubunits around a central pore (11, 15, 16). Each repeat contains six potential transmembrane segments (S1–S6).

A common function of S3 segments from calcium- and sodium-channel proteins is suggested by the extensive amino acid conservation, particularly with respect to negatively charged or polar residues that may be involved in lining a cation-selective channel. S3 segments contributed by each homologous repeat may form an inner bundle of four α-helices, creating the transmembrane pore (15–17).

Here, we describe the chemical synthesis of such a four-helix bundle (15–18): a 9-amino acid template molecule (19) (Lys-Lys-Lys-Pro-Gly-Lys-Glu-Lys-Gly) was used to direct the assembly of four identical 22-mer peptides (18) with sequences representing the S3 segment of the fourth internal repeat of the DHP-sensitive calcium channel (IVS3; Fig. 1*A*). The sequence of IVS3 is homologous in the other repeats and is conserved between skeletal muscle (11) and isoforms of cardiac muscle (8), brain (12), and aorta (13). Empirical secondary structure predictors suggest that the peptide forms an amphipathic α-helix (hydrophobic moment $\mu = 0.23$) (20). A homotetramer of IVS3 (T_4CaIVS3) is, therefore, a plausible model of the proposed heterotetramer forming the pore of the authentic DHP-receptor channel (21).

MATERIALS AND METHODS

Materials. 1-Palmitoyl-2-oleoyl-*sn*-glycerophosphoethanolamine and 1-palmitoyl-2-oleoyl-*sn*-glycerophosphocholine were from Avanti Biochemicals (Alabaster, AL). Other reagents were of the highest purity available commercially.

Molecular Modeling. The model of T_4CaIVS3 was generated by using existing coordinates for sodium-channel S3 homotetramer (22) by specific residue replacements. The INSIGHT and DISCOVER program packages (Biosym Technologies, San Diego, CA) were used on a Silicon Graphics (Mountain View, CA) 4D/210GTXB supercomputing work station (S. Marrer and M.M., unpublished observations).

Synthesis and Purification of Proteins. Four-helix bundle proteins were synthesized by solid-phase methods by simultaneously assembling the four identical peptide blocks after cleavage of the ε-amino groups of template lysines (18). Resin with substitution of 0.15 mmol/g was used (Applied Biosystems). Coupling yields were ≥99.7% for each residue. Protein was cleaved in HF and purified by reversed-phase HPLC. Composition, sequence, and purity were confirmed by amino acid analysis, microsequencing, HPLC, capillary zone electrophoresis, and SDS/PAGE (apparent M_r, ≈9000).

Reconstitution in Lipid Bilayers. Bilayers were formed by hydrophobic apposition of two monolayers at the tip of patch pipettes and studied at 24 ± 2°C (23). Monolayers were spread from a suspension of hexane containing 1-palmitoyl-2-oleoyl-*sn*-glycerophosphoethanolamine/1-palmitoyl-2-oleoyl-*sn*-glycerophosphocholine (4:1; 5 mg/ml) and purified protein at a molar ratio of 1000–10,000:1. Aqueous compartments contained 50 mM divalent salt or 0.5 M monovalent salt and 5 mM Hepes (pH 7.3). In experiments with monovalent cations as charge carriers, 1 mM $BaCl_2$ was included. T_4CaIVS5 recordings were obtained in 50 mM $BaCl_2$.

Data Acquisition and Analysis. Electrical recordings and data processing were performed as described (17, 18). Records were filtered at 1 or 0.5 kHz and digitized at 0.5 or 1 ms per point for analysis and display, respectively, unless indicated otherwise. Single-channel conductances (γ) were calculated from Gaussian fits to current histograms, and open and closed lifetimes were determined from probability density analysis (17, 18); each value was calculated from recordings with ≥300 openings.

EXPERIMENTAL RESULTS AND DISCUSSION

A Bundle of Four Amphipathic α-Helices Is a Plausible Structural Motif for the Calcium-Channel Pore. Low-energy arrangements of α-helical bundles calculated with semiempirical potential energy functions and optimization routines and

The publication costs of this article were defrayed in part by page charge payment. This article must therefore be hereby marked "*advertisement*" in accordance with 18 U.S.C. §1734 solely to indicate this fact.

Abbreviations: γ, single-channel conductance; DHP, dihydropyridine.

‡To whom reprint requests should be addressed.

A TEMPLATE K*KK*PGK*EK*G
IVS3 DPWNVFDFLI VI GS II DVILSE
IVS5 YVALLIVMLFFIYAVIGMQMFGK

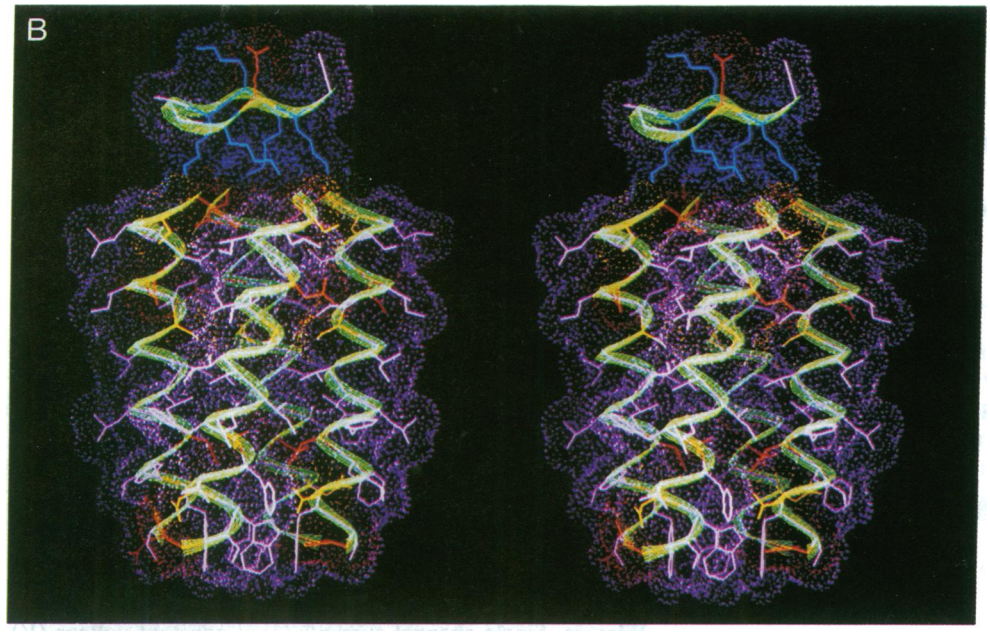

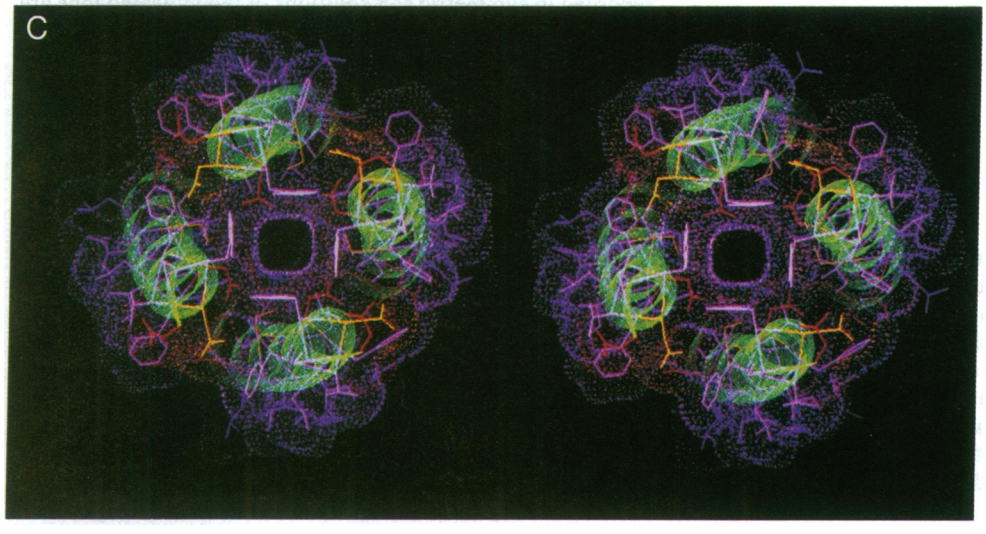

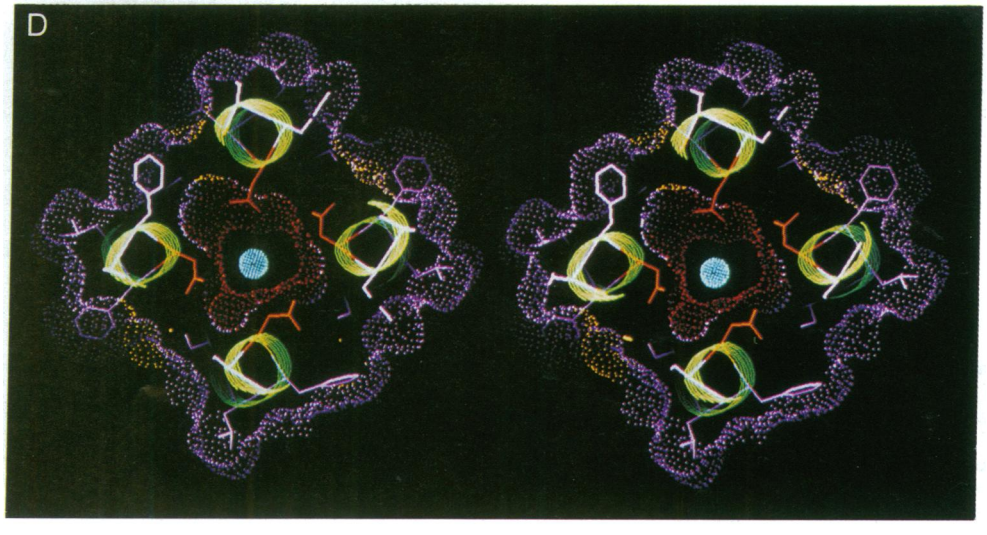

FIG. 1. Computer generated molecular model of the synthetic pore protein. (*A*) Amino acid sequences of template and oligopeptides used to generate the two proteins studied, T_4CaIVS3 and T_4CaIVS5. IVS3 and IVS5 correspond to amino acids 1180–1201 and 1269–1291, respectively (11). Peptides are attached to template lysines, indicated with an asterisk. (*B*) Stereo- side-view of energy optimized parallel tetramer of IVS3 attached to template (T_4CaIVS3). The β-hairpin structure at the top is the template. Color code: green, ribbon representation of the α-carbon backbone; red, acidic; blue, basic; yellow, polar, neutral; purple, lipophilic residues. The solvent accessible surface (magenta, dotted) was calculated with a probe radius of 1.4 Å. The N terminus is at the bottom of the structure and is assigned to the intracellular face of the membrane. (*C*) Stereo- end-view of T_4CaIVS3. The N terminus is in front. The indole groups of Trp-3 form a square vestibule at the pore entry with dimensions 4.5 × 4.5 Å. (*D*) Stereo- end-view of a cross-section at the level of Asp-7 (red dotted surface). A calcium ion is confined within the pore. The distance between opposing carboxylates is 4.2 Å and is the narrowest section of the pore.

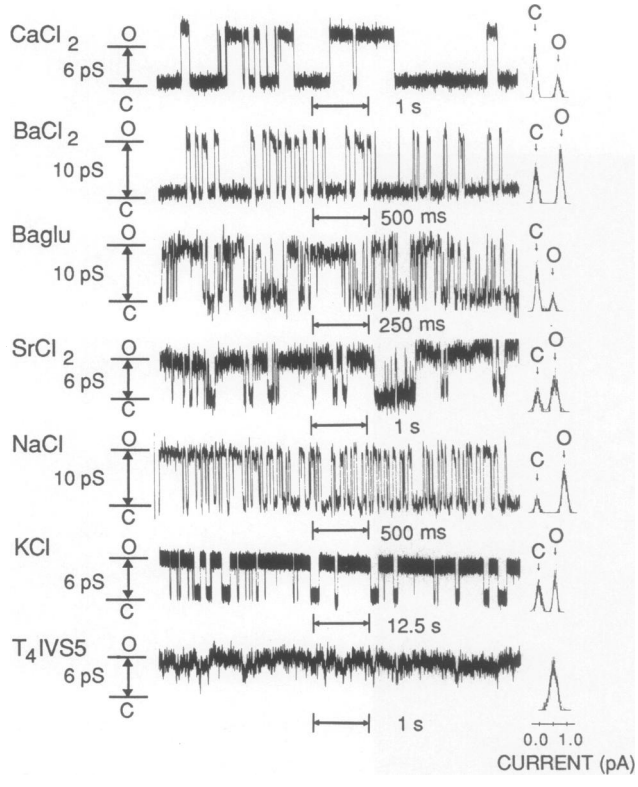

FIG. 2. Single-channel currents from lipid bilayers containing the synthetic T_4CaIVS3 and T_4CaIVS5 proteins in symmetric salt solutions. Currents displayed were recorded at applied voltage $V = 100$ mV except $CaCl_2$ ($V = 120$ mV) and barium 3,3-dimethylglutarate (Baglu; $V = 50$ mV). Note that the channel open time in Baglu is shorter than in $BaCl_2$. T_4CaIVS5 recording was obtained in 50 mM $BaCl_2$. Current histograms generated from segments of records lasting 45, 25, 50, 40, 25, 110, and 45 s, respectively (from top to bottom). C, closed; O, open.

further refined by molecular dynamics (22) are shown in Fig. 1 *B–D*. The side view (Fig. 1*B*) depicts the general structure of the protein: the 9-amino acid template organized as a β hairpin with the four coupling sites at lysine side chains providing spatial organization to the α-helical bundle. The orientation of the free glutamic acid and lysine of the template is opposite that of the four-helix bundle, which is funnel shaped with the narrowest end pointing to the N terminus. The N-terminal residue (Asp-1), which, in the model of the calcium-channel protein, is assigned to the intracellular face of the membrane (11), corresponds to the untethered end of the helices. The helices are parallel and the bundle has a left-handed twist with an interhelical angle of ≈15°. The length of the bundle is sufficient to span the lipid bilayer (32 Å) (22).

Fig. 1*C* displays a projection through the bundle, with the N terminus in front. The solvent accessible surface is shown (dotted) and dimensions are measured at the surface boundaries of the indicated groups. The exterior of the bundle is hydrophobic and the lumen of the pore is lined with polar/neutral residues and two clusters of acidic residues (Asp-7 and Asp-17). At the entry of the pore, a square vestibule with a cross-section of 4.5 Å is formed by tryptophan residues (Trp-3). The shortest distance between the two antiparallel strands of the template β hairpin is ≈4 Å. The pore diameter at its narrowest extent is 4.2 Å and occurs at Asp-7.

Fig. 1*D* shows a transverse section across the bundle depicting approximately one turn of helix bounded between Phe-6 and Leu-9; a calcium ion is confined within the cavity. The four carboxylates of Asp-7 create a ring of negative charge surrounding the calcium ion.

Thus, the bundle of four amphipathic α-helices (T_4CaIVS3) satisfies the structural and energetic requirements for the function of the inner bundle that forms the pore of calcium-channel proteins: it exhibits fourfold symmetry and extensive sequence homology, appropriate pore dimensions, and pore-lining residues, which allow for cation selectivity, including two sequential high-affinity calcium binding sites (Asp-7 and Asp-17).

The Designed Pore Protein Forms Ion Channels in Lipid Bilayers. Single-channel currents (I) at constant voltage (V) recorded in symmetric salt solutions of the indicated ions are shown in Fig. 2. The corresponding current histograms illustrate the occurrence of two distinct states, closed (C) and open (O). γ, calculated from current histograms, is for divalent ions (in 50 mM salt): Ca^{2+}, 7 pS; Ba^{2+}, 10 pS; and Sr^{2+}, 6 pS. γ in $BaCl_2$ and barium 3,3-dimethylglutarate is equivalent, indicating the cation selectivity of the pore. In 0.5 M NaCl and KCl, $\gamma = 11$ and 6 pS, respectively. The apparent selectivity ratio inferred from conductance ratios is $Ba^{2+} > Ca^{2+} > Sr^{2+} > Na^+ > K^+ >> Cl^-$, in agreement with measurements on authentic calcium channels (Table 1).

Sequence Specificity. To assess the specificity of the sequence selected for design of a calcium pore protein, we identified a potential transmembrane segment, IVS5 (Fig. 1*A*), which is hydrophobic ($\mu = 0.07$) and highly conserved, yet is not considered to line an aqueous channel (15, 16, 20). The peptide is predicted to be helical and the tetramer T_4CaIVS5 presumably forms a cluster of α-helices. As shown in Fig. 2 (lowest trace), the synthetic T_4CaIVS5 does not form distinct unitary conductance events characteristic of channel proteins ($n = 9$), but only erratic and fluctuating drifts in

Table 1. Ionic conductance and modulator sensitivity of synthetic and authentic calcium channels

	Conductance, pS			Concentration,† M	
Ion	Synthetic	Authentic	Modulator	Synthetic	Authentic
Ca^{2+}	6.9 ± 0.3 (n = 9)	8	Nifedipine	10^{-7} (n = 6)	10^{-7} (25)
Ba^{2+}	10.2 ± 0.4 (n = 25)	25	Verapamil	10^{-6} (n = 5)	10^{-5} (25)
Sr^{2+}	6.4 ± 0.3 (n = 3)	9	QX-222	10^{-4} (n = 4)	10^{-4} (25)
Na^+	10.9 ± 0.7 (n = 5)	NR	Cd^{2+}	10^{-5} (n = 3)	10^{-5} (26, 27)
K^+	6.1 ± 0.3 (n = 4)	NR	Ca^{2+}	10^{-6} (n = 3)	10^{-6} (27)
			(+)BayK 8644	10^{-7} (n = 4)	10^{-7} (28)
			(−)BayK 8644	10^{-7} (n = 9)	10^{-7} (28)

Conductance values were calculated from Gaussian fits to current histograms. Values are means ± SEM; n denotes number of experiments. Total number of events analyzed is 71,862. Values were obtained with synthetic calcium-channel protein T_4CaIVS3 compared with γ reported for cardiac DHP-sensitive calcium channel (24). γ for divalent (50 mM) or monovalent (500 mM) ions was determined at 100 mV. NR, not reported under comparable conditions.

*γ calculated from slopes of I–V plots in 50 mM chloride (pH 7.4).

†Concentration range at which channel activity is affected by the indicated modulator. Concentration required to increase [(−)BayK 8644] or reduce (all other modulators) activity by ≥80% for experiments with synthetic protein T_4CaIVS3, or as reported in references indicated in parentheses is shown.

membrane current. The current histogram shows a single broad band, in contrast to the two distinct peaks present in recordings obtained with T_4CaIVS3. Apparently, T_4CaIVS5 is incorporated into the bilayer but does not form discrete transmembrane structures. Thus, the single channels recorded with T_4CaIVS3 indicate a requirement for sequence specificity in the design.

Ionic Selectivity and Conduction Through the Synthetic Pore Protein. To establish the selectivity of the protein between cations and anions, *I–V* relations (-100 mV $\leq V \leq 100$ mV) in different salt solutions under symmetric conditions and under single salt concentration gradients were measured. The channel is ohmic in both conditions. Transference numbers for Ca^{2+} (0.91 ± 0.07; $n = 4$) and Ba^{2+} (0.95 ± 0.08; $n = 3$), calculated from reversal potentials obtained under 10-fold concentration gradients of $CaCl_2$ or $BaCl_2$, indicate that the current-carrying species is the cation.

γ increases with salt concentration and approaches saturation. The apparent salt concentration at which γ is half-maximal is 21 mM for Ba^{2+}, 18 mM for Ca^{2+}, and 14 mM for Sr^{2+}, in fair agreement with values of authentic calcium channels (24). Thus, the synthetic channel protein forms cation-selective pores that exhibit saturation consistent with the occurrence of low-affinity (mM) binding sites for divalent cations within the pore lumen.

Pharmacological Specificity. Calcium channels are receptors for a variety of drugs, including many DHP derivatives (e.g., nifedipine) and other channel blockers (e.g., verapamil and local anesthetics), which are of clinical importance. The significance of DHP compounds is underscored by the availability of enantiomers that act as activators (agonists) or blockers (antagonists) of calcium channels (29). This pharmacological specificity provides a valuable tool to assess the integrity of the designed pore protein.

As shown in Fig. 3, nifedipine, verapamil, and QX-222, a quaternary ammonium derivative of the local anesthetic lidocaine, block ion conduction through the synthetic pore protein. Fig. 3 shows segments of single-channel recordings obtained before (traces A) and after (traces B and C) addition of blocker; recordings obtained in the presence of modulator are selected to qualitatively display channel activity. Blocking is initially manifested as increased occurrence of brief openings or fast interruptions (flickering) of the long-lived open state, whereas γ is unaltered. This is evident in trace B from each group of recordings. The pattern of channel activity is progressively dominated by the infrequent occurrence of very brief events. Eventually the open-channel lifetime cannot be resolved, leading to an apparent reduction of γ (trace C). As summarized in Table 1, blocking is effective at similar concentrations in both synthetic and authentic calcium channels.

The Synthetic Calcium Channel Is Blocked by Cd^{2+} and Ca^{2+}. A key property of calcium channels is their susceptibility to block by polyvalent metal ions such as Cd^{2+}; divalent ion currents through synthetic channels are also blocked by micromolar Cd^{2+} (Fig. 3). Ca^{2+} blocks monovalent currents through authentic calcium channels; as shown in Fig. 3, Ca^{2+} blocks K^+ currents through the synthetic pore protein. Long openings dominate before addition of Ca^{2+}, which immediately results in the occurrence of brief openings and a shortening of the long open time. Accordingly, the designed protein contains intrapore Ca^{2+} binding sites of high affinity (μM; Table 1), in accordance with authentic calcium channels (1, 26, 27).

The Activity of DHP on the Synthetic Pore Protein Is Stereospecific. Antagonist and agonist effects of DHP enantiomers are displayed in Fig. 4. After addition of (+)BayK 8644 (antagonist), a drastic reduction in the number of openings and in the open lifetime is evident. Conversely, the agonist effect of the (−)-enantiomer of BayK 8644 is indicated by an increased open probability and a prolongation of channel open time. Hence, the stereospecific activity of DHP on the synthetic channel matches that exerted on authentic channels (for review, see refs. 1 and 2).

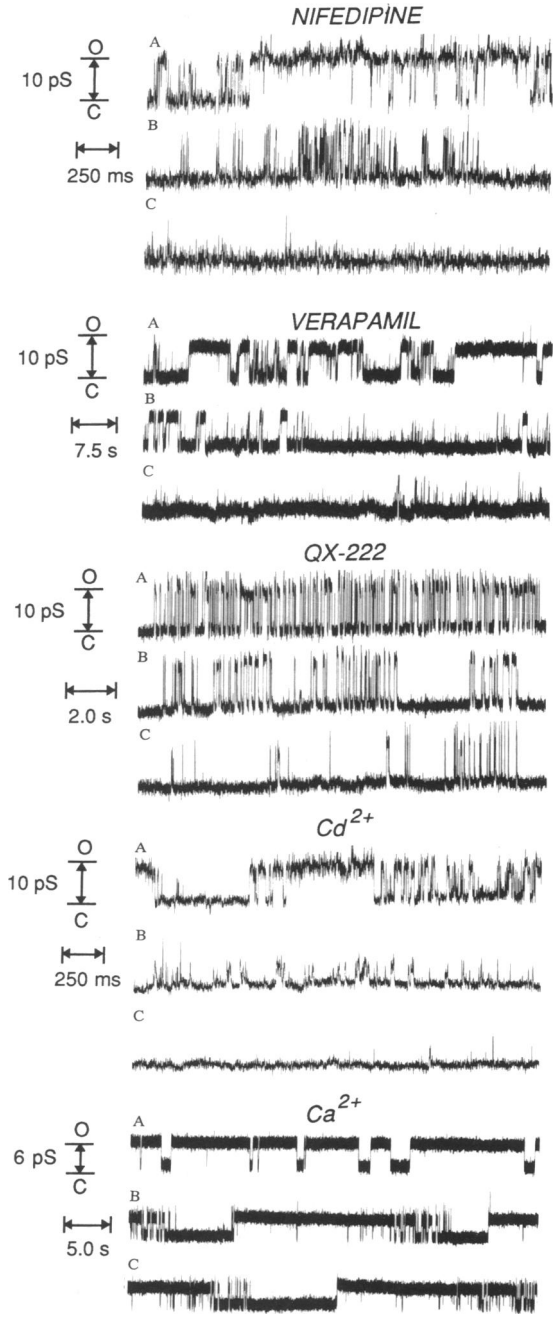

FIG. 3. Blocking of ion conduction through the synthetic calcium channel. Single-channel currents were from lipid bilayers containing T_4CaIVS3 in symmetric 50 mM $BaCl_2$ (first four groups of recordings) or symmetric 0.5 M KCl (last group of recordings). Current traces are before (traces A) and after (traces B and C) addition of blocker. Currents were recorded at $V = 100$ mV except for nifedipine ($V = 50$ mV). Nifedipine: trace A, control; traces B and C, recorded 1 and 2 min after addition of 100 nM nifedipine; open channel probability (Po) reduced from 60% to ≤2%. Verapamil: trace A, control; traces B and C, recorded 1 min after addition of 2.4 and 4.8 μM verapamil, a reduction of Po from 65% to ≤2%. QX-222, trace A, control; traces B and C, recorded 1 and 5 min after addition of 250 μM QX-222; Po was reduced from 50% to ≤5%. Cd^{2+}: trace A, control; traces B and C, 1 and 3 min after addition of 10 μM $CdCl_2$. Po was reduced from 40% to ≤2%. Records were filtered at 400 Hz for display. Ca^{2+}: trace A, control, in 0.5 M KCl; traces B and C, consecutive records 3 min after addition of 1 mM $CaCl_2$; Po was reduced from 74% to ≤5% after 10 min. Stock solutions (10 mM in ethanol) of nifedipine were stored refrigerated in the dark. Other conditions are as described (23). C, closed; O, open.

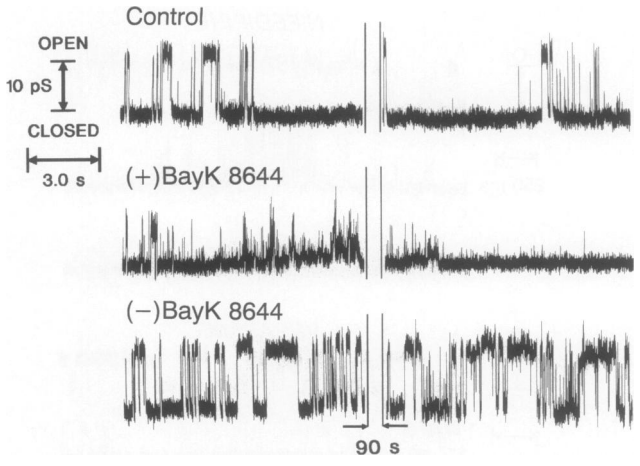

FIG. 4. Stereoselective modulation of the synthetic calcium channel by antagonist and agonist DHP derivatives. Single-channel currents from lipid bilayers containing T_4CaIVS3 in symmetric 50 mM $BaCl_2$ before (Control; $V = 100$ mV) and after addition of drug. Recordings in the presence of (+)BayK 8644 [200 nM; open channel probability (Po) $\leq 2\%$; $V = 50$ mV; filtered at 300 Hz] and (−)BayK 8644 (100 nM; Po $\geq 50\%$; $V = 100$ mV) start 1 and 5 min after addition of compound, respectively. The display is interrupted (90 s) to show the persistence of the drug effect. Other conditions are as described (23).

A Plausible Unifying Structural Motif for the Pore of Cation-Selective Channels. A search for sequences compatible with a three-dimensional structure used as pathway for Ca^{2+} led to the identification of IVS3. The designed bundle of four identical α-helices representing IVS3 features a narrowest cross-section of 4.2 Å, which agrees with the geometric constraints of the DHP-sensitive calcium channel (1, 2). The finding that affinity for Ca^{2+} measured by block (≤ 5 μM) and by saturation (18 mM) are different indicates that at least two Ca^{2+} binding sites are associated with the synthetic pore protein, a biophysical hallmark of the authentic protein (1, 2). The pharmacological specificity exhibited by the synthetic channel demonstrates that the design mimics the inner bundle that lines the calcium channel.

The extensive sequence homology between calcium and sodium channels at the level of S3 supports the notion that a bundle of four S3 α-helices may represent a unifying structural motif for the inner bundle of this superfamily of voltage-gated, cation-selective channels (15–17, 22). The "selectivity filter," a key property of cation-selective channels (2), may correspond to the ring of conserved aspartic acid residues exposed to the luminal face of the pore (Fig. 1*D*). The proposal that such a structural motif represents a molecular blueprint for the pore structure of this superfamily of channel proteins is further substantiated by the comparable sensitivity of authentic sodium and calcium channels and of the synthetic pore protein to drugs, such as local anesthetics (30, 31), and the stereoselective action of BayK 8644 enantiomers (32, 33). Potential binding sites for verapamil (34) and nitrendipine (35) were assigned to a sequence succeeding the IVS6 repeat in the predicted cytoplasmic domain of the calcium-channel protein. The availability of the structure model (Fig. 1) and of the synthetic pore protein should prove valuable in assessing the functional role of key residues and should facilitate the conceptual design of drugs that alter the pore by blocking it from the aqueous pathway or via the hydrophobic access to the protein from the bilayer interior.

We thank S. Marrer for molecular modeling, T. Iwamoto for protein synthesis and purification, J. Rivier for constructive criticism, and A. Scriabine and A. Schwartz for BayK 8644. This work was supported by grants from the National Institutes of Health (GM-42340 and MH-44638 to M.M. and GM-43617 to J.M.T.), the Office of Naval Research (N00014-89-J-1469 to M.M.), the Department of the Army Medical Research (DAMD17-89-C-9032 to M.M.), and by a Research Scientist Award to M.M. from the Alcohol, Drug Abuse and Mental Health Administration (MH-00778).

1. Hess, P. (1990) *Annu. Rev. Neurosci.* **13,** 337–356.
2. Tsien, R. W., Hess, P., McCleskey, E. W. & Rosenberg, R. L. (1987) *Annu. Rev. Biophys. Biophys. Chem.* **16,** 265–290.
3. Triggle, D. J., Langs, D. A. & Janis, R. A. (1989) *Med. Res. Rev.* **9,** 123–180.
4. Ellis, S. B., Williams, M. E., Ways, N. R., Brenner, R., Sharp, A. H., Leung, A. T., Campbell, K. P., McKenna, E., Koch, W. J., Hui, A., Schwartz, A. & Harpold, M. M. (1988) *Science* **241,** 1661–1664.
5. Ruth, P., Röhrkasten, A., Biel, M., Bosse, E., Regulla, S., Meyer, H. E., Flockerzi, V. & Hofmann, F. (1989) *Science* **245,** 1115–1118.
6. Jay, S. D., Ellis, S. B., McCue, A. F., Williams, M. E., Vedvick, T. S., Harpold, M. M. & Campbell, K. P. (1990) *Science* **248,** 490–492.
7. Catterall, W. A., Seagar, M. J. & Takahashi, M. (1988) *J. Biol. Chem.* **263,** 3535–3538.
8. Mikami, A., Imoto, K., Tanabe, T., Niidome, T., Mori, Y., Takeshima, H., Narumiya, S. & Numa, S. (1989) *Nature (London)* **340,** 230–233.
9. Tanabe, T., Beam, K. G., Powell, J. A. & Numa, S. (1988) *Nature (London)* **336,** 134–139.
10. Perez-Reyes, E., Kim, H. S., Lacerdan, A. E., Horney, W., Wei, X., Rampe, D., Campbell, K. P., Brown, A. M. & Birnbaumer, L. (1989) *Nature (London)* **340,** 233–236.
11. Tanabe, T., Takeshima, H., Mikami, A., Flockerzi, V., Takahashi, H., Kangawa, K., Kojima, M., Matsuo, H., Hirose, T. & Numa, S. (1987) *Nature (London)* **328,** 313–318.
12. Snutch, T., Leonard, J. P., Gilbert, M. M., Lester, H. A. & Davidson, N. (1990) *Proc. Natl. Acad. Sci. USA* **87,** 3391–3395.
13. Koch, W. J., Hui, A., Shull, G. E., Ellinor, P. & Schwartz, A. (1989) *FEBS Lett.* **250,** 386–388.
14. Biel, M., Ruth, P., Bosse, E., Hullin, R., Stühmer, W., Flockerzi, V. & Hofmann, F. (1990) *FEBS Lett.* **269,** 409–412.
15. Montal, M. (1990) *FASEB J.* **4,** 2623–2635.
16. Greenblatt, R. E., Blatt, Y. & Montal, M. (1985) *FEBS Lett.* **193,** 125–134.
17. Oiki, S., Danho, W. & Montal, M. (1988) *Proc. Natl. Acad. Sci. USA* **85,** 2393–2397.
18. Montal, M., Montal, M. S. & Tomich, J. M. (1990) *Proc. Natl. Acad. Sci. USA* **87,** 6929–6933.
19. Mutter, M., Hersperger, R., Gubernator, K. & Müller, K. (1989) *Proteins: Struct. Funct. Genet.* **5,** 13–21.
20. Eisenberg, D. (1984) *Annu. Rev. Biochem.* **53,** 595–623.
21. Grove, A., Tomich, J. M. & Montal, M. (1990) *Soc. Neurosci. Abstr.* **16,** 957.
22. Oiki, S., Madison, V. & Montal, M. (1990) *Proteins: Struct. Funct. Genet.* **8,** 226–236.
23. Suarez-Isla, B. A., Wan, K., Lindstrom, J. & Montal, M. (1983) *Biochemistry* **22,** 2319–2323.
24. Hess, P., Lansman, J. B. & Tsien, R. W. (1986) *J. Gen. Physiol.* **88,** 293–319.
25. Palade, P. T. & Almers, W. (1985) *Pflügers Arch.* **405,** 91–101.
26. Lansman, J. B., Hess, P. & Tsien, R. W. (1986) *J. Gen. Physiol.* **88,** 321–347.
27. Rosenberg, R. L., Hess, P. & Tsien, R. W. (1988) *J. Gen. Physiol.* **92,** 27–54.
28. Kass, R. S. (1987) *Circ. Res. Suppl.* **61,** 1–5.
29. Vaghy, P. L., Williams, J. S. & Schwartz, A. (1987) *Am. J. Cardiol.* **59,** 9A–17A.
30. Josephson, I. R. (1988) *J. Mol. Cell. Cardiol.* **20,** 593–604.
31. Bolger, G. T., Marcus, K. A., Daly, J. W. & Skolnick, P. (1987) *J. Pharmacol. Exp. Ther.* **240,** 922–930.
32. Yatani, A. & Brown, A. M. (1985) *Circ. Res.* **57,** 868–875.
33. Yatani, A., Kunze, D. L. & Brown, A. M. (1988) *Am. J. Physiol.* **23,** H140–H147.
34. Striessnig, J., Glossman, H. & Catterall, W. A. (1990) *Proc. Natl. Acad. Sci. USA* **87,** 9108–9112.
35. Regulla, S., Schneider, T., Nastainczyk, W., Meyer, H. E. & Hofmann, F. (1991) *EMBO J.* **10,** 45–49.